POLITECNICO DI TORINO
Repository ISTITUZIONALE

Investigation of surface shot blasting of AlSi10Mg and Ti6Al4V components produced by powder bed fusion technologies

Original
Investigation of surface shot blasting of AlSi10Mg and Ti6Al4V components produced by powder bed fusion technologies / Calignano, F., Mercurio, V., Rizza, G., Galati, M.. - In: PRECISION ENGINEERING. - ISSN 0141-6359. - (2022). [10.1016/j.precisioneng.2022.07.008]

Availability:
This version is available at: 11583/2970330 since: 2022-10-03T15:00:02Z

Publisher:
Elsevier

Published
DOI:10.1016/j.precisioneng.2022.07.008

Terms of use:

This article is made available under terms and conditions as specified in the corresponding bibliographic description in the repository

Publisher copyright

(Article begins on next page)

28 November 2026

Investigation of surface shot blasting of AlSi10Mg and Ti6Al4V components produced by powder bed fusion technologies

Flaviana Calignano*, Vincenza Mercurio, Giovanni Rizza, Manuela Galati

Department of Management and Production Engineering (DIGEP) - Integrated Additive Manufacturing Center (IAM) - Politecnico di Torino, Corso Duca Degli Abruzzi, 24 - 10129 Torino, Italy

*Correspondence: flaviana.calignano@polito.it; Tel.: +39 011 090 7218

Abstract

Metal additive manufacturing (AM) is constantly expanding thanks to the freedom to create complex, light, and high performing geometries within the limits of the processing itself. As-built AM parts, especially when using powder bed fusion (PBF) processes, exhibit surface imperfections and defects leading to a remarkably irregular morphology that can significantly affect the product aesthetical and mechanical performance. Because of that, the part post-processing is a crucial step. Shot blasting is a simple and fast-finishing process commonly used in the AM supply chain to remove residual sintered particles attached to the component surface and reduce the surface roughness. This study investigates the shot blasting processes performed on AlSi10Mg and Ti6Al4V parts produced using laser-PBF (L-PBF) and electron beam-PBF (EB-PBF), respectively, considering the great geometric variability that a single component designed for AM can have in surface texture and geometries. Test artifacts were therefore devised with internal channels enclosed in the reticular structures and inclined flat surfaces to evaluate what happens in the external surface, internal channels, and reticular structures at the level of roughness and accuracy when these are simultaneously affected by the flow of abrasives. The effect of glass and zirconia microspheres and their combination on the surface roughness are analyzed. The results show a reduction of surface roughness up to approximately 38% for L-PBF and 82% for EB-PBF parts without altering their geometrical characteristics and processing the part for less than one minute.

Keywords: laser powder bed fusion; electron beam melting; surface roughness; additive manufacturing; shot blasting: shot peening; aluminium alloy, titanium alloy; glass microsphere; zirconia

1. Introduction

Surface texture metrology was born to verify compliance with specific surface requirements that a component must possess to perform certain functions. It can also be considered a means of acquiring information on the physical phenomena that occur during the production process with additive technologies. This is possible through examining the surface characteristics generated by the process and, proceeding backwards, through the complex network of cause-effect relationships involving physical phenomena [1], hydrodynamics, and circulation of Marangoni [2] and variable control process. Therefore, balling defects, satellites, overhangs from down-skin surfaces, staircase defects, and partially fused particles piled up on the rippled outer surface can be found [3,4]. In general, the surface texture consists of all the aforementioned irregularities present on the surface of the AM metal parts, whose origins must be fully understood before any surface treatment. Surface structure metrology thus becomes a powerful exploration tool, increasing process knowledge and ultimately enabling the creation of improved additive manufacturing (AM) processes capable of producing parts that conform to specifications [5]. In fact, AM is now able to produce high-quality metal alloy parts that are increasingly used for structural aerospace applications. This is possible because, thanks to the evolution, for example, of the types and powers of the lasers [6], the parts are now completely dense with few pores and mechanical characteristics equivalent to or superior to a forged part. However, these parts generally exhibit inadequate and poor surface quality in the as-built configuration. Surface imperfections due to the choice of melting process parameters, part geometry, surface orientation with respect to construction direction, and support structure design can greatly affect surface quality leading to significantly uneven surface morphology [7–10]. This high surface roughness can considerably deteriorate the performance of products, imposing a limit on possible applications. Much effort has recently been devoted to developing post-treatment to

improve the surface quality of additively produced metallic parts. Therefore, the search for surface post-processing solutions has become an area of growing interest as an effective tool for improving the functionality and durability of metal components produced via AM technologies. A wide variety of surface post-treatments have been applied to AM metal parts. These treatments are mainly classified according to the intrinsic characteristics of the applied technology and final effects on the workpiece surface. In this way, treatments are based on mechanical, thermal, chemical and electrochemical interaction. Each finishing process has limitations and complexities which impact on design. Treatments based on mechanical interaction mainly include CNC machining [11], shot peening [12–14], vibration polishing [15,16], sandblasting [17], fluid bed [18–21] and hydrodynamic cavitation-based abrasives [22,23]. Except for the latter, it can be observed that these surface treatments present severe limitations relating to the physical access of tools and abrasive means in parts with complex shapes such as those obtainable through AM. Treatments based on thermal interaction mainly refer to laser polishing processes [24–26]. Regardless of the specific configuration of the process, the laser sources and the materials treated, laser polishing provides, through remelting and ablation mechanisms, a certain amount of heat on the surface to favour its smoothing. Compared to other surface finishing technologies, laser polishing is characterized by a process having greater input control due to the precise characteristics of the laser source and process parameters. This aspect is desirable for a surface smoothing process applied to a non-uniform textured surface such as those obtained through metallic AM processes. However, these polishing techniques are hampered due to the need for access for the laser to the internals of complex components. Therefore, the number of possible applications in AM is small. However, when applicable, laser polishing represents a solution that guarantees a final high surface quality. Chemical and electrochemical-based surface treatments represent one of the most promising solutions to obtain a homogeneous smoothing of the complex parts with internal channels and reticular structures. Electrochemical polishing (electropolishing) has acquired notoriety in recent years for products made of AM as it is considered an ideal method to improve surface roughness

and, simultaneously, significantly improve electrical conductivity [27]. Surface polished products are currently treated with hazardous chemical solutions [28,29]. In particular, phosphoric and sulfuric acid mixtures represent a plurality of these acid electropolishing treatments in pure metals and alloys [27,30]. Acidic solutions provide the metal with a mirror finish at the expense of hydrogen contamination [27,31]. Removal of hydrogen contamination generally involves using high-temperature treatments above 800 °C for several hours under vacuum [32].

In AM powder bed fusion (PBF) processes, cleaning the component from sintered particles is essential before any surface treatment. In particular, for the metal PBF process that uses the laser as a heat source (laser powder bed fusion, L-PBF), the part cleaning aims only to remove the sintered powder particles that stick on the surface. Shot blasting and shot peening are the most common abrasive blasting processes used for this purpose. The processes are highly similar. Both are based on throwing a stream of abrasive material at high-pressure against the component surface. However, the different process parameters, such as the operation time, generated different effects on the surface. In the case of shot blasting, the process is performed using a fast stream of abrasive material. The tiny abrasive media acts slowly, chipping away at the "dirty" surface layer to reveal a "cleaner" layer underneath. Shot peening instead involves a cold dynamic plastic treatment of the surface. The process also modifies the residual surface stresses [33–36]. The typical abrasives for cleaning the samples by shot blasting are glass or ceramic particles. The abrasive material depends on the desired level of final surface roughness. Differently from the L-PBF process, the electron beam powder bed fusion (EB-PBF) is a hot process [37]. Due to the high environmental temperature, the parts are surrounded by partially sintered powder particles that form the so-called “powder cake” at the end of the production. After the production, the part needs to be free from the sintered cake, and unused sintered particles in the cake need to be recovered. This operation consists of the sandblasting process performed in a powder recovery system (PRS). The abrasive used during this operation is the same powder used in the process. In this way, the loose powder can be easily reused for the next production [38–40]. The sandblasting performed after an EB-PBF with

the PRS is part of the standard procedure of this process with the sole purpose of cleaning the components produced and not with the idea of affecting their surface roughness. The typical surface roughness of as-built EB-PBF is over 20 µm [41]. Therefore, in EB-PBF, subsequent operations are needed to improve the surface quality. The shot blasting process could represent a simple and rapid route to improve the surface roughness of both PBF processes.

This study investigates shot blasting processes in detail by analyzing the effect of using glass and ceramic, and a mixture of them in equal percentages on complex additively manufactured surfaces. To define a unique protocol for metal PBF processes, the finishing tests were performed, including internal channels and thin structures and the most common materials produced by L-PBF and EB-PBF, which correspond to AlSi10Mg and Ti6Al4V, respectively. Al-Si-Mg casting alloys are characterized by having a low density combined with good mechanical properties and excellent castability [42]. Within this family of alloys, AlSi10Mg is a hypoeutectic alloy with a wide diffusion in the L-PBF process thanks to its narrow solidification interval, which reduces the susceptibility to hot cracking during rapid cooling [43,44]. It is an alloy used in a wide range of applications, including the aerospace and automotive industries, to various engineering parts [45]. Ti6Al4V alloy occupies nearly half the market share of titanium products used in the world today thanks to characteristics such as high resistance and fracture toughness, biocompatibility and excellent corrosion resistance. Initially developed for aeronautical structural applications, this lightweight yet strong alloy saves weight in highly loaded structures and is therefore suitable for jet engines, gas turbines and prosthetics [46–49]. In the case of EB-PBF, the high environment temperature makes it possible to produce as-built components in Ti6Al4V with a lamellar microstructure $\alpha + \beta$ free of residual stresses and with similar strength and ductility value to traditionally fabricated [50]. Having different hardness characteristics, these alloys allow an in-depth analysis of the effects of the abrasives and their mixture on the surface. The analysis of surfaces from different PBF processes allows for analysis of the finishing protocol also on extremely different as-built surface roughness as well. Furthermore, this study aims to investigate

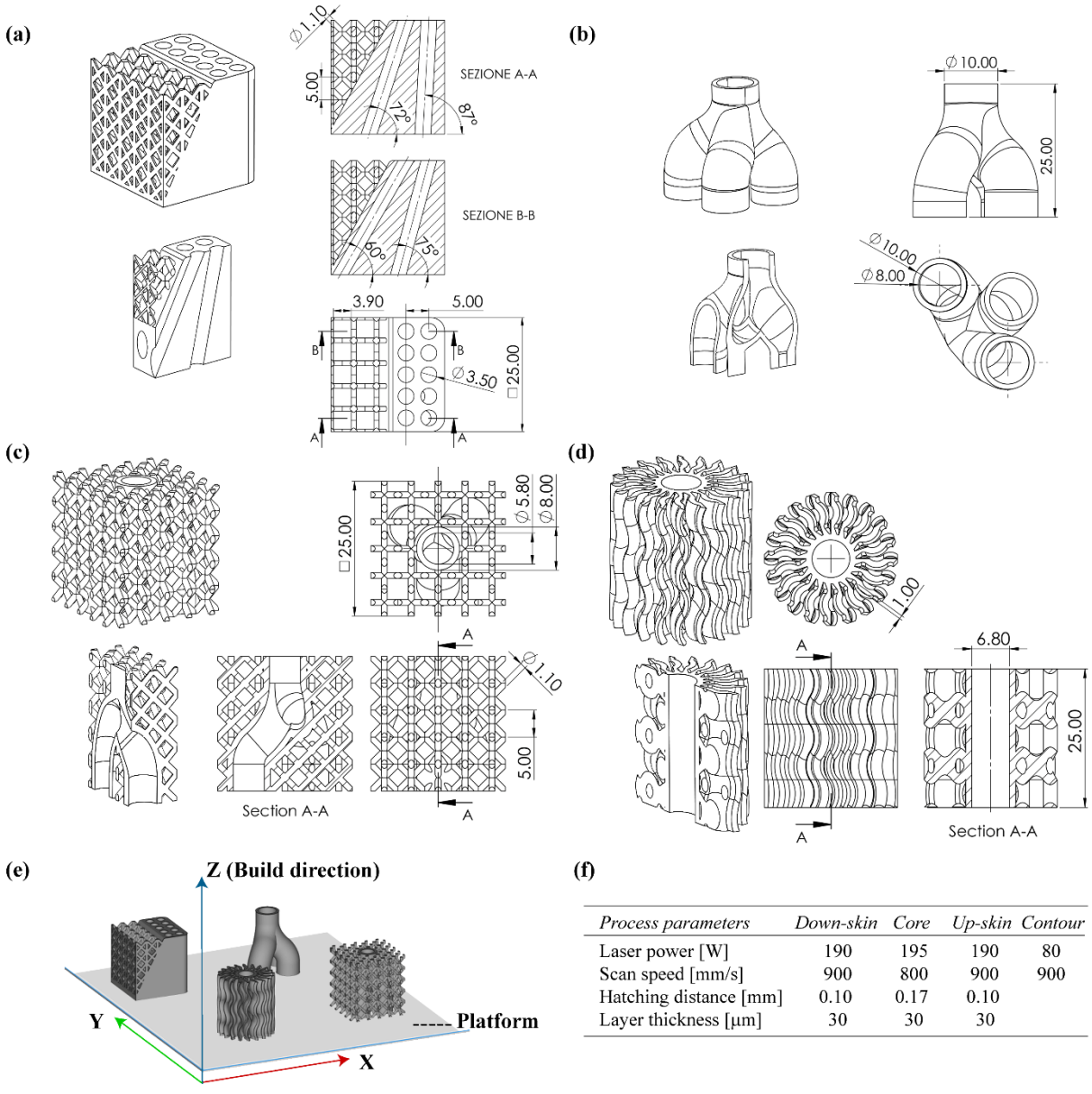
the shot blasting processes performed on AlSi10Mg and Ti6Al4V parts, considering the geometric variability that a single component designed for AM can have in surface texture and geometries. The studies on roughness reduction for additive components aim above all, to investigate the effect on the individual geometries or areas of the components. In this case, test artifacts were devised with internal channels enclosed in the reticular structures and inclined flat surfaces to evaluate what happens in the external surface, internal channels, and reticular structures in terms of roughness but also of precision when these are simultaneously affected by the flow of abrasives. In fact, the abrasive will not only hit the area where the jet is directed, but the abrasives will also affect the neighbouring areas that may have geometric characteristics and need for accuracy different from the affected area.

2. Materials and methods

2.1 Test artifacts

Five test artifacts for AlSi10Mg alloy were designed to represent the main geometrical characteristics of the components designed for AM, i.e. lightweight structures (e.g. reticular structures and wall thicknesses ≥ 1mm), internal channels and free forms (Figure 1). The reason for the choice of these geometries was to evaluate how shot blasting could affect components consisting of internal channels and thin external geometries that simultaneously receive the same flow of media being monolithic pieces. In particular, T_a1 (Figure 1a) consists of a cube with a side dimension of 25 mm with ten internal channels of 3.5 mm diameter with a progressively greater inclination with respect to the vertical axis. In particular, the inclinations of the channels range from 3 degrees to 30 degrees in 3 degrees increments. The area not affected by the canals has been lightened by means of a reticular structure. The cellular unit of the reticular structure is a cube of 5 mm per side and the diameter of the cylindrical elements is 1.1 mm. T_a2 (Figure 1b) was designed with free-form channels with external and internal diameters of 10 mm and 8 mm respectively. The height of the sample is 25 mm. T_a3 (Figure 1c) also has free-form internal channels, but in this case

they are drowned in a 25 mm side reticular cube. The external and internal diameters measure respectively 8 mm and 5.8 mm and the dimension of the reticular cell unit is the same as that of T_a1. Sample T_a4 is designed as a part of a heat exchanger equipped with fins with a particular surface, as shown in Figure 2d. The height of the sample is 25 mm, the central channel has external and internal diameters respectively of 24 mm and 6.8 mm, and the fins have a thickness of 1 mm. The test artifacts were produced using EOSINT M270 Dual Mode machine with optimized process parameters [51]. Figure 1e shows the build direction.



Process parameters	*Down-skin*	*Core*	*Up-skin*	*Contour*
Laser power [W]	190	195	190	80
Scan speed [mm/s]	900	800	900	900
Hatching distance [mm]	0.10	0.17	0.10	
Layer thickness [μm]	30	30	30	

Figure 1. Test artifacts produced in AlSi10Mg alloy: (a) T_a1, (b) T_a2, (c) T_a3, (d) T_a4; (e) orientation in the build platform, (f) process parameters used to build test artifacts.

Ti6Al4V test artefact were produced using Arcam A2X machine with a standard theme for the hatch and the contour [9,41]. The geometry of the test artifact is fan-shaped with different surfaces with different angles measured with respect to the build platform [41]. There are 4 different zones (Figure 2): zone 1 consisting of five external up-skin surfaces (us_e), zone 2 formed by five internal down-skin surfaces (ds_i), zone 3 formed by the five internal surfaces of up-skin (us_i), and zone 4 formed by five lower external surfaces of down-skin (ds_e). These surfaces are parallel to each other to obtain a constant cross-section during the melting of the layer to ensure an even distribution of the heat generated during the melting phase.

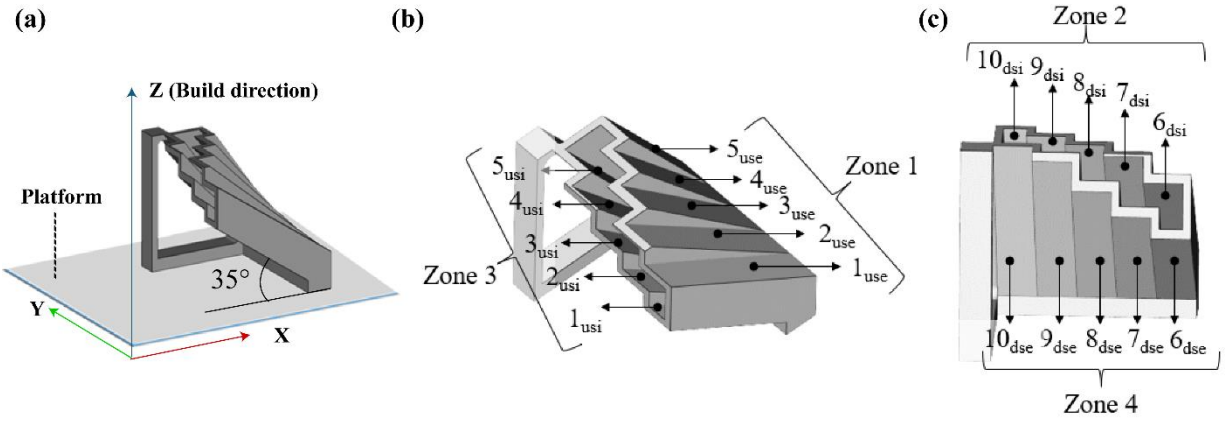


Figure 2. Test artifacts produced in Ti6Al4V alloy: (a) orientation in the build platform, (b) up-skin and (c) down-skin zones.

The surface of zone 1 marked 1 is inclined 35 degrees with respect to the start plate, while the other surfaces are sloped in 5 degrees increments to 55 degrees. After production, the partially sintered powder is removed from the components by shot blasting in the PRS at a pressure of 4.5 bar.

2.2 Methodology

2.2.1 Shot blasting: abrasives and Almen test

Norblast SD9 shot blasting machine was used with two different media, microspheres of glass and zirconia (Table 1), tested in three different conditions:

- 100% glass
- 100% zirconia
- 50% glass and 50% zirconia (named "mix").

There are four properties of an abrasive that contribute to surface profile depth: size, shape, hardness, and density. These properties of the abrasives used are shown in Table 1. Particle sizes are commonly classified by mesh sizes, often given as a range, for example, 75-150 mesh (210-89 μm). This indicates that 95% of the mix will fall through a 75 mesh but not pass through the 150. Shapes are classified according to angularity. The spherical shape leaves imprints regular, spherical in shape, while angular shapes of the abrasives would lead to irregular that could act as points of ignition of the fracture. Hardness determines whether an abrasive particle can etch a particular type of substrate. The hardness of an abrasive is frequently communicated according to the Mohs' hardness scale. The scale ranges from 1 to 10, with 1 being the softest (talc) and 10 being the hardest (diamond).

Media type	**Shape**	**Diameter [μm]**	**Specific gravity [g/cm^3]**	**Hardness [Mohs]**	**Chemical analysis [%]**	**Cost [€/kg]**
Glass	Spherical	75-150	2.5	5-5½	SiO_2: < 75%; NaO_2 < 15%; CaO <10%; MgO <5%	1.04 – 3.67
Zirconia	Spherical	63-125	3.8	6-7½	ZrO_2: 60-70%; SiO_2: 28-33%; Al_2O_3: <10%	9.97 – 34.59

Table 1. Nominal size range, physical properties, chemical composition, and cost of the abrasives used for shot blasting treatment.

The intensity of shot blasting, as it happens for shot peening, is measured on special unified specimens that allow the control of the main parameters of surface deformation of the piece and, therefore, the correct adjustment of the machine. The intensity measure is expressed in Almen degrees [52,53]. For each abrasive, the variation of the arc height with the shot blasting time was

measured, obtaining the saturation curve (Figure 3). The type N Almen strip samples (conformed to SAE J443 [54]) were shot blasted using a pressure of 6 bar. The distance from the tip of the nozzle to the specimen is 30 mm. With increasing time (Figure 4), the peening coverage increases (Figure 4a, 4c and 4d) and there is a reduction in the contribution of the arc height (Figure 4b, 4d, and 4f), due to the plastic deformation of the surface, determining the shape of the intensity curves of the shot blasting. The reduced effect of the glass microspheres, visible in the lower intensity and curvature of the strips, can already indicate the little effect it will have on components with high roughness and hard material. Furthermore, these will certainly chip quickly, generating a less sweet and more angular effect on the surface. On the other hand, zirconia has a high intensity that generates many valleys on the surface. The mix produces more deformation than glass but is reduced compared to zirconia.

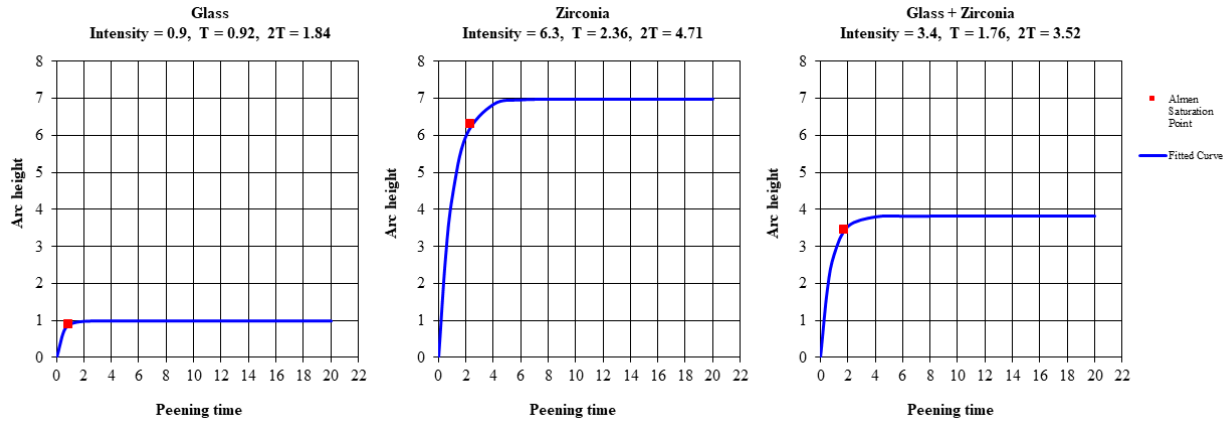
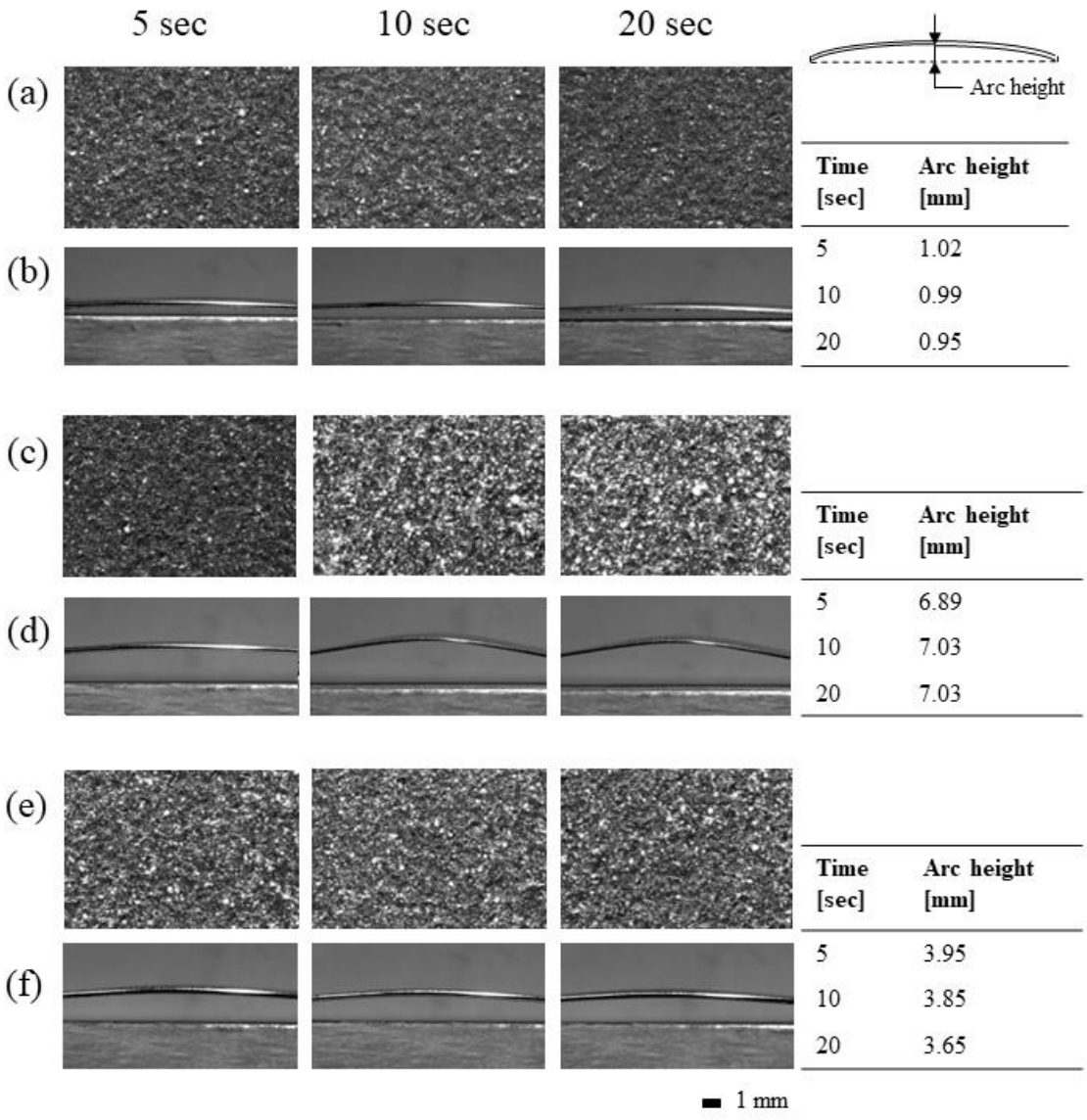


Figure 3. Saturation curves for Almen strips (SAE/AISI 1070 cold rolled steel).



Time [sec]	Arc height [mm]
5	1.02
10	0.99
20	0.95

Time [sec]	Arc height [mm]
5	6.89
10	7.03
20	7.03

Time [sec]	Arc height [mm]
5	3.95
10	3.85
20	3.65

Figure 4. Coverage and arc heights in three different peening times for Almen strip: (a) and (b) glass microsphere; (b) and (c) zirconia microspheres; (d) and (e) mix.

After observing these results, it was decided to shoot the samples for 10 seconds at 90 degrees and another 10 seconds at 45 degrees. In particular, the external surfaces were positioned perpendicular to the jet by moving back and forth for 10 seconds and then inclined by 45 degrees. When the abrasive grain hits the surface of the support at angles less than 60 degrees, a small volume of material is eroded, depending on the chosen angle [55]. Thus, traces of micro-cuts remain on the surface based on the hardness of the material with respect to the abrasive. Conversely, with an impact angle greater than 60°, the abrasive grain penetrates the surface leading to the extrusion of

the material at the periphery of the notching area [55]. From the Almen test it was possible to obtain the maximum intensity and the time to reach it. Starting from this, the first inclination of 90 degrees was adopted, which allows to considerably reduce the ridges. However, since, as previously mentioned, it could lead to the formation of further depressions, subsequently using the 45 degree inclination, an attempt is made to standardize the previously bombed area.

For the internal channels, the sample was positioned so that the axis of the channel was parallel to the jet and then tilted 45 degrees relative to it, constantly rotating it so that the jet met the entire internal surface. Furthermore, since the channels of the samples T_a2 and T_a3 have a free-form shape, during shot blasting, one side is momentarily closed with a support surface so that the abrasive hitting the surface is internally reflected, producing certain turbulence in that area which is far from the jet and therefore could be less affected by the effect of the stream itself.

2.2.2 Roughness measurement

The surface roughness, in terms of values of roughness average (R_a) and the average maximum height of the profile (R_z), of the sample were measured as-built, after stress relieving, and after shot blasting with the use of SM Metrology Systems RPT80 tester with a diamond stylus of a radius of 2 µm and resolution of 0.001µm (Figure 5). The measurement distance was 4.8 mm, and a 0.8 mm cut-off filter was used. The choice of parameters to be adopted was made considering that to characterize the surface texture of the PBF processes, small measurement areas are sufficient (about 2.5 mm^2) but not less than the dimensions of the large irregularities [56,57]. From the measurement of the dimensions of the typical surface defects of PBF technologies, it is possible to identify an optimal dimension of cut-off wavelength. In particular, it is possible to analyze the surface texture using short wavelengths in the presence of loose and/or partially fused particles and long wavelengths in the case of defects such as the staircase effect, semi-welded structures, and balling melts [56]. In this study, therefore, parameters were chosen that have been shown in the literature

[58,59] to be optimal for representing the surface of the two PBF metal technologies. Five measurements were collected in different directions on each surface, and the arithmetic mean of the measurements was used for the analysis. The Stereo Microscope Leica S9i was used for the stereo microscope images.

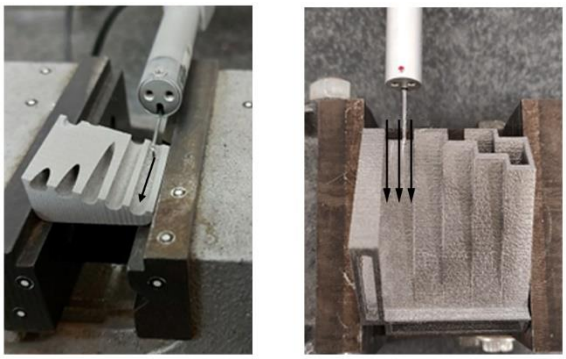


Figure 5. Roughness measurement direction for (a) internal channels of the test artifacts made with L-PBF and (b) EB-PBF test artifacts.

3. Results and discussion

3.1 AlSi10Mg test artifact

The surface roughness was measured as-built, after stress-relieving (SR), and after shot-blasting with the three different combinations of media (Figure 6 and Table S1 (see Supplementary Information)). The surface roughness analysis showed that the treated surface has a higher roughness value ranging, in terms of R_a, from a minimum of about 5% for the T_a3 sample to a maximum of about 23% for the T_a4 sample compared to their respective as-built samples. Even at the R_z level, the SR samples show higher values between 5% (sample T_a1) and 14% (sample T_a4) than the as-built values. Due to the nature of the powder bed process, as-built samples have unfused and partially fused powder particles. Once the SR treatment has been carried out at 300°C for 2 hours, the surface of the thermally treated sample has a structure consisting of partially sintered spheroids. The increase in surface roughness may be due not only to the partial melting of the

particles but also to oxidation due to the treatment carried out not in a vacuum. As soon as the metal comes into contact with air, an aluminum oxide film quickly forms at any temperature. Heat treatments, such as stress relieving at 300 °C, induce a change in the morphology of the passive film, i.e. they increase the thickness of the layer and the crystallinity of the oxide, and produce a porous and micro-cracked structure, which has, for example, a resistance less corrosion than amorphous film [60]. The mechanical actions of shot blasting smooth the original rough surface and remove the formed film both during the process itself and after the heat treatment.

There are no significant differences between the external and internal roughness values of the channels. Considering the R_z values (Figure 6), and, therefore the maximum roughness, it is possible to note that for the sample T_a1 the roughness is reduced by using the mix compared to the single abrasives, but the variability is observable by the greater dimension of the interquartile range increases. An increase in variability is also noted on the T_a3 sample, which has, however, a lower roughness than the T_a2 sample despite the channels being similar. This may be due to the variation in the size of the diameters. 50% of the roughness values of the T_a4 sample obtained after peening with zirconia remain within the interquartile range of the as-built (1st Quartile (Q_1) 38.20 µm - 3rd Quartile (Q_3) 52.25 µm) but with less variability. Using glass, the values and variability are reduced (Q_1 30.80 µm - Q_3 38.70 µm). The mixture of media remains around the values obtained with the glass, further reducing the variability (Q_1 33.86 µm – Q_3 38.45 µm).

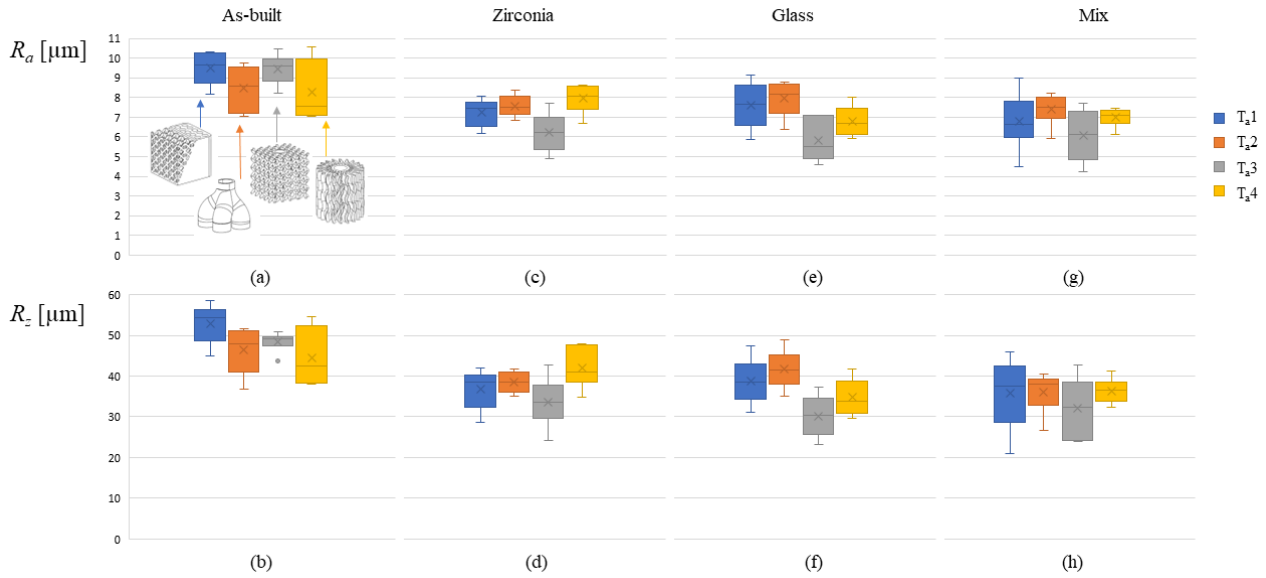


Figure 6. Box plot of the median and interquartile range for R_a [µm] and R_z [µm] measured for AlSi10Mg samples. The "x" sign in the box represents the mean value. Surface roughness values are measured in the direction indicated in Figure 5a.

To better understand the different roughness reductions, in particular in the T_a2 and T_a3 samples, the internal channels for T_a1, T_a2, and T_a3 have been divided into two features: the first which refers to the area called down-skin and the second to the area called up-skin (Figure 7). Generally, the down-skin area has a greater roughness than the one up-skin as they are areas that grow on the powder supported by supports or, for some angles, self-support. In the latter case, when the laser melts the powder, the heat is dissipated differently between the melting area and the surrounding powder. The speed of heat conduction, being considerably lower than the conduction in the solid, induces a melting pool larger than the already melted layer [7]. As the powder particles are packed randomly, inducing varying thermal conductivity, the melting pools sink deep into the powder, and with the pressure of the recoater blade and capillary forces in play, they solidify into an extremely rough surface with large deformities called "dross" [61]. The formation of dross causes both great surface roughness and a poor geometric precision of the overhanging surfaces. The roughness measurement after shot blasting did not show any differences between the two areas. The flow lines, remaining substantially parallel to the generatrices of the cavity walls, cause the shot

suspended in the air flow to cross the cavity without adequately striking the surface to significantly reduce its roughness but in an adequate way to remove the unmelted particles that they will be greater in the down-skin area. This action, therefore, partially reduces the peaks. The 45 degrees inclination creates a series of incident and overturning impacts between the walls of the cavity and the media, which tend to smear the peaks and thus reduce the valleys.

If it is considered the roughness with respect to the geometrical shape of the test artefacts, it is possible to see that when an internal channel is surrounded externally by reticular structures, such as the T_a3 sample, the mixture, and glass similarly reduce the roughness. However, glass microspheres have a greater interquartile range.

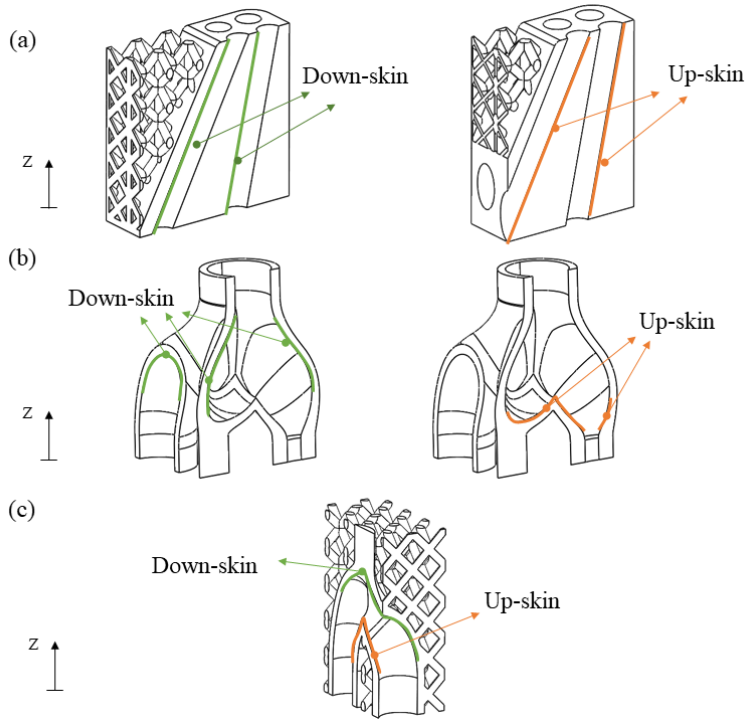


Figure 7. Down-skin and up-skin zones in (a) T_a1, (b) T_a2, and (c) T_a3 samples. T_a2, and T_a3 have the same internal channel.

This reduction in roughness in the internal channels did not lead to a high dimensional variation of thin structures such as struts (Table 2 and Figure 8). If the roughness reduction is compared with the value of the geometric dimensions of the struts, it is possible to note that the mix allows to get

closer to the nominal value, if already through the process parameters the values are close to those of the CAD model.

	xy-plane [mm]		zx-planes [mm]		zy-plane [mm]	
Nominal	1.10	1.56	1.10	1.56	1.10	1.56
As-built	1.12	1.57	1.11	1.57	1.13	1.55
Zirconia	1.08	1.55	1.06	1.53	1.05	1.54
Glass	1.12	1.56	1.09	1.55	1.11	1.55
Mix	1.10	1.56	1.08	1.56	1.09	1.55

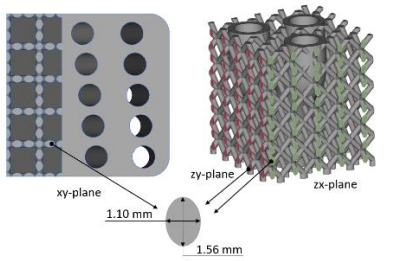


Table 2. Geometrical dimensions of the struts and CAD models for the AlSi10Mg samples. Standard deviation: ± 0.03 mm.

Analyzing the external surfaces, the struts, and the internal channels (Figure 8), it is possible to notice an equal effect of the media starting from the area, the shape and the ease or otherwise of reaching all the areas of the components during shot blasting. In particular, there are slight differences between the surfaces without and with SR attributable to the thermal process. As for welding, the thermal SR process improves the overall quality of the melt by reducing distortions and deformations that can derive from the stress generated by the continuous rapid thermal variations that occur during the melting and cooling process. The surface roughness induces local geometric discontinuities that act as stress concentrators [62]. Therefore, by heating the material, the thermal SR process provides an energy value that induces a redistribution of any imperfections deriving from selective melting. This, combined with the non-partially melted powder on the surfaces, could explain the visual reduction of the laser traces on the surfaces. Glass microspheres tend to create a scaly surface in vertical walls due to the material ductility. At the level of up-skin surfaces, they manage to homogenize the surface while releasing wavy areas. Zirconia creates larger valleys in vertical and up-skin surfaces due to the hardness of the abrasive relative to the component material. The mix allows a compromise between the two effects due to glass and zirconia.

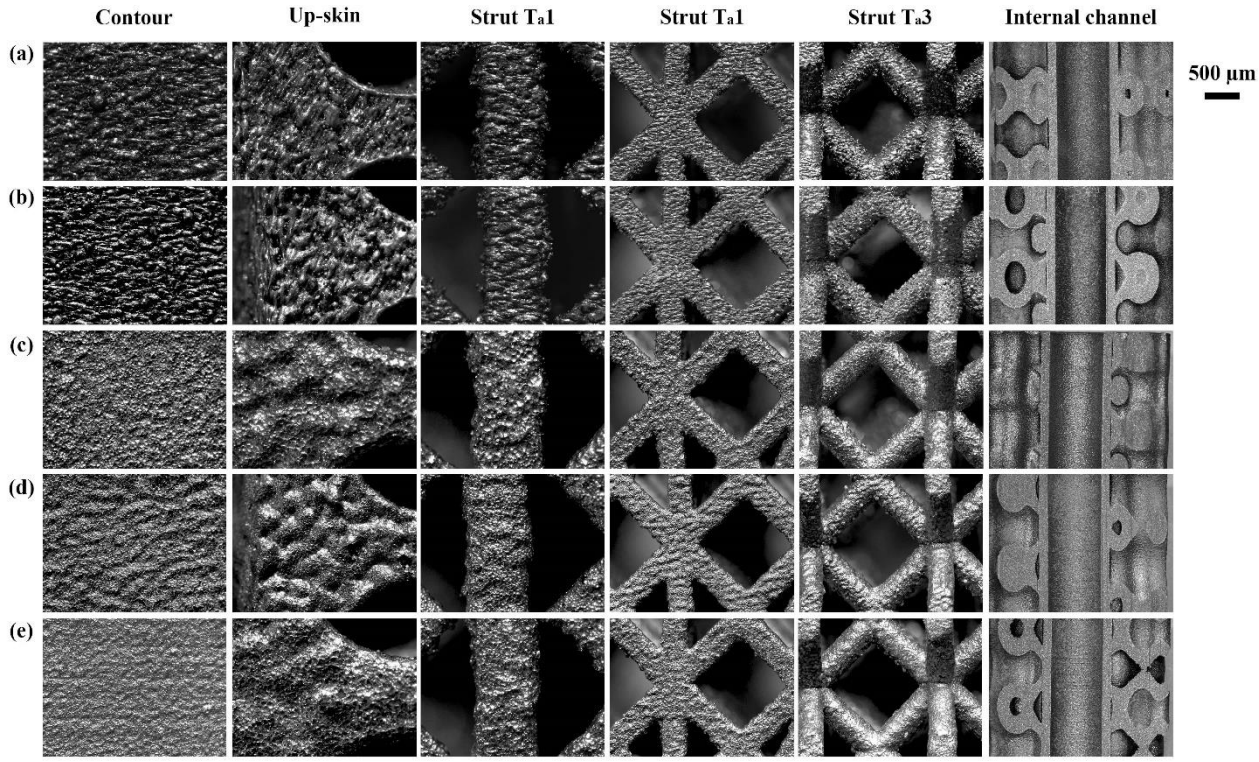


Figure 8. Stereo microscope images for AlSi10Mg samples: (a) As-built without SR and (b) after SR; shot blasting with (c) glass, (d) zirconia, and (e) mix media.

3.2 Ti6Al4V specimens

Figure 9 and Table S2 (see Supplementary Information) report the surface roughness measured as-built and after shot blasting. The as-built surface refers to the part surface after the operation by PRS because, as above mentioned, this operation is mandatory to free the part from the sintered cake. With respect to the laser process, the standard EB-PBF cycle does not include any stress-relieving or subsequent shot blasting operation to improve the surface roughness.

In the as-built condition, lower roughness values are observed in the internal areas (zones 2 and 3) than in the external ones (Figure 9). Therefore, by observing the values on the individual faces in more detail (Table S2), it can be seen that the roughness for the up-skin areas in general increases from 35 degrees to 55 degrees (faces from 1 to 5) for the external surfaces (zone 1) while in those interiors (zone 3) from 55 degrees to 35 degrees is reduced, in agreement with Galati et al. [41]. For the down-skin, going from 55 degrees to 35 degrees (faces from 10 to 6), in the internal surfaces

(zone 2), the roughness decreases, while for the external ones, it increases (zone 4). This may be due to two factors: powder preheating and PRS blasting. In contrast to the L-PBF process, in the EB-PBF process, the powder bed is preheated before the melting. Firstly, a preheating step slightly sinters the entire powder bed. Then, a second preheating is performed in an area corresponding to an offset of the area to be melted and increase the sintered level locally. The higher connectivity of the sintered powder compared to the loose powder induces an improvement in the thermal conductivity of the powder bed. Since zones 2 and 3 are located at a close distance immersed in layers of powder brought to a certain degree of temperature, it can be deduced that a better diffusion of heat is generated. This is a desirable condition when melting overhanging surfaces with no prior molten material underneath them since, as previously mentioned, the thermal energy imparted during melting is not dissipated as quickly by the powder as it would be by the previously molten solid material. Considering the PRS, internally, the titanium particles arrive with a certain pressure on the sintered powder and on the walls, which slowly clean themselves and rebound in the area around them against the surfaces. This produces a reduction of the superficial ridges. Externally, the particles do not flip against the surfaces but are dispersed in the air. The as-built roughness is greater in the up-skin for angles less than 55 degrees because the surface exposed in each layer to the effect of shot blasting is greater. Considering that the samples were manufactured using layer thicknesses of 50 µm, the exposed up-skin surface on each layer will range from a maximum of 0.087 µm for 35 degrees angles to a minimum of 0.061 µm for 55 degrees angles. Therefore, the average of the particles will have a greater impact surface for smaller angles. The combination of these two effects is verified by the roughness values of the vertical internal surfaces found in the part where the component rests on the platform. The roughness is equal to 23.22 µm ± 2.66 µm and 106.04 µm ± 12.46 µm for R_a and R_z, respectively. Therefore, this area has values more similar to the external surface at the level of R_a but as R_z of the same order as that obtained in the internal surfaces. Considering the range of titanium particles used for PRS that goes from 45 to 105 µm (the same used in the process), if the pressure used with the PRS were increased compared to the 4.5 bar

used, there could be an increase in the depth of the valleys as these are already present at the pressure used. It, therefore, becomes essential to consider a phase after the PRS based on the use of shot blasting.

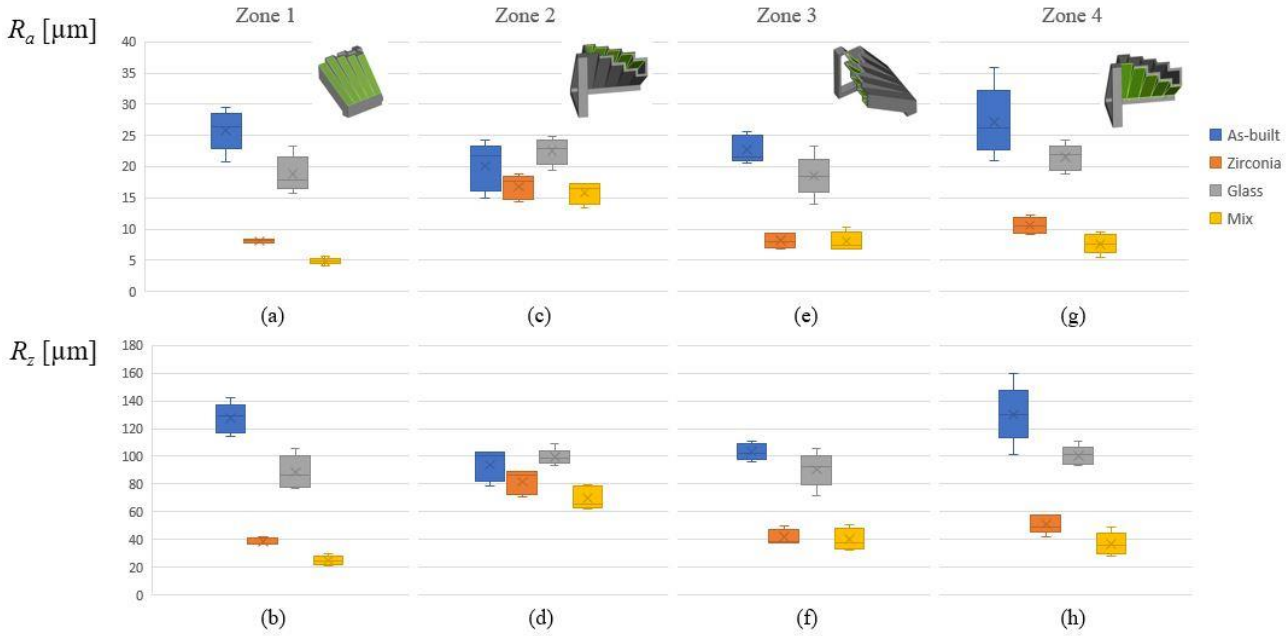


Figure 9. Box plot of the median and interquartile range for R_a [µm] and R_z [µm] for the Ti6Al4V sample. The "x" sign in the box represents the mean value. Surface roughness values are measured in the direction indicated in Figure 5b.

Observing in fact the average values of the different zones after shot blasting, it is possible to notice a high reduction in roughness if zirconia or mixture are used. In particular, in zone 1, although the use of zirconia or mix leads to a high decrease of the interquartile range, the use of the mix reduces roughness by almost half compared to zirconia alone. The effect of the glass microspheres on roughness is very low (Figures 10b and 10f). To distinguish if this effect was due to the type of abrasive or the time used, the time was increased from 20 seconds (10 seconds with the perpendicular flow and 10 seconds with 45 degrees inclination) to 40 seconds up to 1 minute without having any variation (Figure 10b and f). Unlike glass microspheres, a reduction in roughness in 20 seconds was achieved with zirconia. By increasing the time, "pitted" areas were created on the surface, which, therefore, even if they reduced the roughness, damaged the surface more (Figure 10c and g). The results obtained on the external surfaces of up-skin (us_e) after shot

blasting with the mix showed a uniform reduction (Figure 10d and h) regardless of the degree of initial roughness due to the different inclination. In the mix, the presence of glass is as if it reduces the aggressive effect of zirconia alone, allowing for more uniform surfaces. Observing the profiles of the surfaces, it can be seen that both the zirconia and the mix are able to brush the ridges, partly covering the valleys. In the case of the mix, there is a greater periodicity and uniformity of the effect on the various layers.

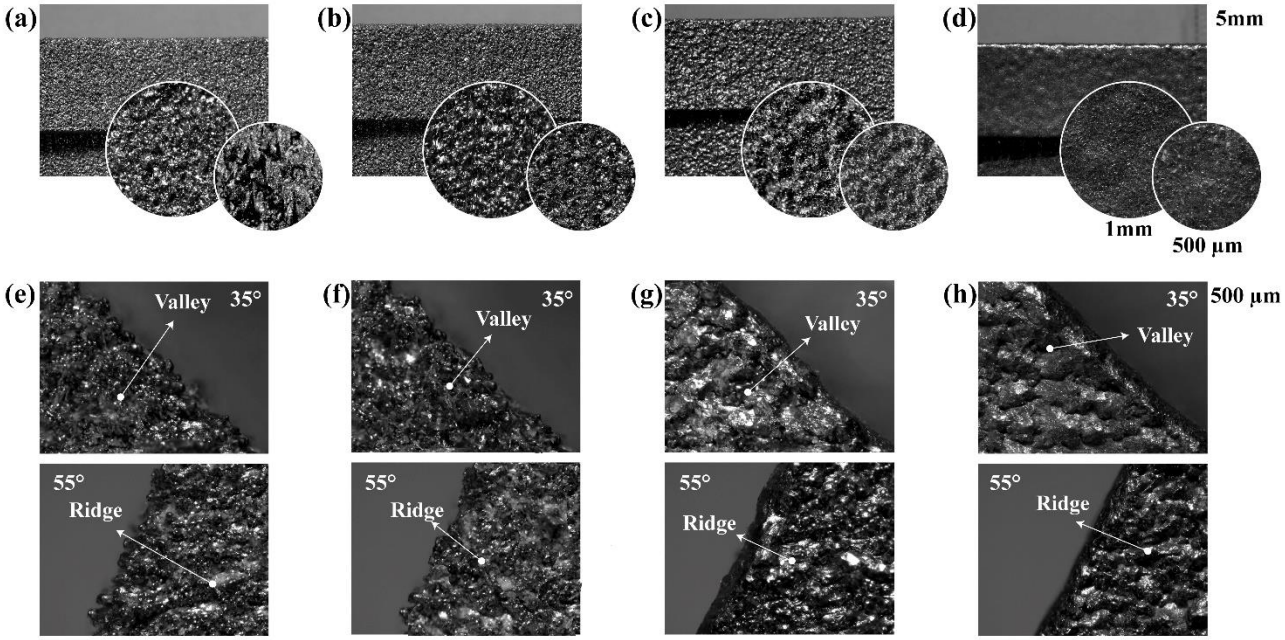


Figure 10. Ti6Al4V samples. Top view: (a) As-built sample; after shot blasting with (b) glass microspheres, (c) zirconia, and (d) mix. Side view: (e) As-built sample; after shot blasting with (f) glass microspheres, (g) zirconia, and (h) mix.

3.3 Comparison

From the analysis of the results on the individual materials and related processes, it is clear that the mix showed excellent powder removal, preservation of dimensional accuracy, and reduction of ridges.

In the case of aluminum, the effect obtained from zirconia is extremely pronounced, leading to the reduction of the peak but also to the formation of valleys. The appearance of these valleys may be

associated with some mechanical effect more typical of shot peening operations and undesirable with the respect of applying only a surface treatment that modifies the surface roughness.

A general rule is to use an abrasive harder than the material being shot-peened. In this case, on the Mohs scale, the hardness of aluminum is 2.75 Mohs, lower by about 118% than zirconia (Table 1). Given the material ductility, the pressure used, and therefore the intensity, in this case, is excessive. However, in the case of titanium samples, this pressure helps better clean surfaces from the sintered powders and significantly reduces the roughness peaks. The hardness of titanium is 6 Mohs, therefore in line with the general rule.

Although glass has a higher relative hardness than aluminum, a beneficial effect on the surface has been observed when cleaning AlSi10Mg samples produced for L-PBF. However, the particles tend to degrade easily, which is readily visible in Ti6Al4V for EB-PBF. When the glass particles collide with the hard surface of the titanium, they are scratched and lose their spherical shape. The lower hardness of glass with respect to titanium explains the almost negligible effects on the Ti6Al4V samples. With a hardness lower than titanium, the shot blasting with glass cannot reduce the roughness using zirconia.

The combined effect of the two abrasives shows a more uniform reduction of the ridges in both materials. The percentage of reduction of the presence of zirconia in the mix allows having a less accentuated bubble effect on the aluminum similar to the phenomenon observed when the pressure was reduced using only the zirconia.

4. Conclusion

The study was conducted on the effects of two abrasives and the combination of these for the reduction of the surface roughness of the components produced by L-PBF and EB-PBF technologies. From the results obtained, it can be deduced that:

- glass microspheres affect the roughness of the aluminum alloy but not on the titanium alloy. In particular, if the material is very hard and/or the roughness is high, as in the case of EB-PBF, the effect of the glass microspheres is very mild;
- Zirconia considerably reduces the roughness both in the laser and in the electron beam melted parts. However, at a pressure of 6 bar, at the distance of 30 mm between the piece and the nozzle tip, and for times longer than 20 seconds, the zirconia can damage the surface, creating more or less deep grooves depending on the hardness of the component material;
- Using a mix between 50% glass and 50% zirconia allows for combining the advantages of both abrasives.

A significant result is a high reduction obtained on the components produced with EB-PBF, suggesting the introduction of shot blasting in the process supply chain. Shot blasting can be considered a crucial phase of the additive process for both processes, both for preparing the samples for subsequent finishing operations if very low values or more planar surfaces are required and for final finishing, if the roughness results are obtained are suitable for the application required.

References

[1] DebRoy T, Wei HL, Zuback JS, Mukherjee T, Elmer JW, Milewski JO, et al. Additive manufacturing of metallic components – Process, structure and properties. Prog Mater Sci 2018. https://doi.org/10.1016/j.pmatsci.2017.10.001.

[2] Huang Y, Fleming TG, Clark SJ, Marussi S, Fezzaa K, Thiyagalingam J, et al. Keyhole fluctuation and pore formation mechanisms during laser powder bed fusion additive manufacturing. Nat Commun 2022. https://doi.org/10.1038/s41467-022-28694-x.

[3] Wang L zhi, Wang S, Wu J jiao. Experimental investigation on densification behavior and surface roughness of AlSi10Mg powders produced by selective laser melting. Opt Laser Technol 2017. https://doi.org/10.1016/j.optlastec.2017.05.006.

[4] Shiyas KA, Ramanujam R. A review on post processing techniques of additively manufactured metal parts for improving the material properties. Mater Today Proc 2021. https://doi.org/10.1016/j.matpr.2021.03.016.

[5] Townsend A, Senin N, Blunt L, Leach RK, Taylor JS. Surface texture metrology for metal additive manufacturing: a review. Precis Eng 2016. https://doi.org/10.1016/j.precisioneng.2016.06.001.

[6] Lee H, Lim CHJ, Low MJ, Tham N, Murukeshan VM, Kim YJ. Lasers in additive manufacturing: A review. Int J Precis Eng Manuf - Green Technol 2017. https://doi.org/10.1007/s40684-017-0037-7.

[7] Calignano F. Investigation of the accuracy and roughness in the laser powder bed fusion process. Virtual Phys Prototyp 2018. https://doi.org/10.1080/17452759.2018.1426368.

[8] Sadeghi E, Pant P, Jafari R, Peng RL, Karimi P. Subsurface grain refinement in electron beam-powder bed fusion of Alloy 718: Surface texture and oxidation performance. Mater Charact 2020. https://doi.org/10.1016/j.matchar.2020.110567.

[9] Galati M, Minetola P, Rizza G. Surface roughness characterisation and analysis of the Electron Beam Melting (EBM) process. Materials (Basel) 2019. https://doi.org/10.3390/ma12132211.

[10] Yasa E, Deckers J, Kruth JP. The investigation of the influence of laser re-melting on density, surface quality and microstructure of selective laser melting parts. Rapid Prototyp J 2011. https://doi.org/10.1108/13552541111156450.

[11] Du W, Bai Q, Zhang B. A Novel Method for Additive/Subtractive Hybrid Manufacturing of Metallic Parts. Procedia Manuf 2016. https://doi.org/10.1016/j.promfg.2016.08.067.

[12] Calignano F, Manfredi D, Ambrosio EP, Iuliano L, Fino P. Influence of process parameters on surface roughness of aluminum parts produced by DMLS. Int J Adv Manuf Technol 2013. https://doi.org/10.1007/s00170-012-4688-9.

[13] Maamoun A, Elbestawi M, Veldhuis S. Influence of Shot Peening on AlSi10Mg Parts Fabricated by Additive Manufacturing. J Manuf Mater Process 2018. https://doi.org/10.3390/jmmp2030040.

[14] AlMangour B, Yang JM. Improving the surface quality and mechanical properties by shot-peening of 17-4 stainless steel fabricated by additive manufacturing. Mater Des 2016. https://doi.org/10.1016/j.matdes.2016.08.037.

[15] Gumpinger J, Brandão AD, Beevers E, Rohr T, Ghidini T, Beretta S, et al. Expression of Additive Manufacturing Surface Irregularities through a Flaw-Based Assessment. Struct. Integr. Addit. Manuf. Parts, 2020. https://doi.org/10.1520/stp162020180098.

[16] Prochaska S, Hildreth O. Effect of chemically accelerated vibratory finishing on the corrosion behavior of Laser Powder Bed Fusion 316L stainless steel. J Mater Process Technol 2022;305:117596. https://doi.org/10.1016/J.JMATPROTEC.2022.117596.

[17] Bernevig-Sava MA, Stamate C, Lohan NM, Baciu AM, Postolache I, Baciu C, et al. Considerations on the surface roughness of SLM processed metal parts and the effects of subsequent sandblasting. IOP Conf. Ser. Mater. Sci. Eng., 2019. https://doi.org/10.1088/1757-899X/572/1/012071.

[18] Atzeni E, Barletta M, Calignano F, Iuliano L, Rubino G, Tagliaferri V. Abrasive Fluidized Bed (AFB) finishing of AlSi10Mg substrates manufactured by Direct Metal Laser Sintering (DMLS). Addit Manuf 2016. https://doi.org/10.1016/j.addma.2016.01.005.

[19] Hassanin A El, Troiano M, Silvestri AT, Contaldi V, Scherillo F, Solimene R, et al. Fluidised bed machining of metal additive manufactured parts. AIP Conf. Proc., 2019. https://doi.org/10.1063/1.5112685.

[20] Hassanin A El, Troiano M, Silvestri AT, Contaldi V, Scherillo F, Solimene R, et al. Influence of abrasive materials in fluidised bed machining of AlSi10Mg parts made through

selective laser melting technology. Key Eng. Mater., 2019. https://doi.org/10.4028/www.scientific.net/KEM.813.129.

[21] Kum CW, Wu CH, Wan S, Kang CW. Prediction and compensation of material removal for abrasive flow machining of additively manufactured metal components. J Mater Process Technol 2020. https://doi.org/10.1016/j.jmatprotec.2020.116704.

[22] Nagalingam AP, Yuvaraj HK, Yeo SH. Synergistic effects in hydrodynamic cavitation abrasive finishing for internal surface-finish enhancement of additive-manufactured components. Addit Manuf 2020. https://doi.org/10.1016/j.addma.2020.101110.

[23] Sanders D, Soyama H, De Silva C. Use of Cavitation Abrasive Surface Finishing to Improve the Fatigue Properties of Additive Manufactured Titanium Alloy Ti6Al4V. SAE Tech. Pap., 2021. https://doi.org/10.4271/2021-01-0024.

[24] Yung KC, Zhang SS, Duan L, Choy HS, Cai ZX. Laser polishing of additive manufactured tool steel components using pulsed or continuous-wave lasers. Int J Adv Manuf Technol 2019. https://doi.org/10.1007/s00170-019-04205-z.

[25] Temmler A, Liu D, Preußner J, Oeser S, Luo J, Poprawe R, et al. Influence of laser polishing on surface roughness and microstructural properties of the remelted surface boundary layer of tool steel H11. Mater Des 2020. https://doi.org/10.1016/j.matdes.2020.108689.

[26] Tian Y, Gora WS, Cabo AP, Parimi LL, Hand DP, Tammas-Williams S, et al. Material interactions in laser polishing powder bed additive manufactured Ti6Al4V components. Addit Manuf 2018. https://doi.org/10.1016/j.addma.2017.12.010.

[27] Karim WO, Juma JA, Omer KM, Salih YM, Hama Aziz KH, Aziz SB. Electropolishing and Mirror-like preparation of titanium in choline chloride-ethylene glycol mixture liquid. Electrochemistry 2020. https://doi.org/10.5796/electrochemistry.20-00038.

[28] CVETKOVIĆ VS, VUKIĆEVIĆ NM, JOVIĆEVIĆ N, STEVANOVIĆ JS, JOVIĆEVIĆ JN. Aluminium electrodeposition under novel conditions from AlCl3–urea deep eutectic solvent at room temperature. Trans Nonferrous Met Soc China (English Ed 2020. https://doi.org/10.1016/S1003-6326(20)65257-8.

[29] Abdel-Fattah TM, Loftis JD, Mahapatro A. Ionic Liquid Electropolishing of Metal Alloys for Biomedical Applications. ECS Trans 2019. https://doi.org/10.1149/1.3298949.

[30] Hou Y, Li R, Liang J. Simultaneous electropolishing and electrodeposition of aluminum in ionic liquid under ambient conditions. Appl Surf Sci 2018. https://doi.org/10.1016/j.apsusc.2017.11.034.

[31] Andrade LS, Xavier SC, Rocha-Filho RC, Bocchi N, Biaggio SR. Electropolishing of AISI-304 stainless steel using an oxidizing solution originally used for electrochemical coloration. Electrochim Acta 2005. https://doi.org/10.1016/j.electacta.2004.11.007.

[32] Kityk A, Protsenko V, Danilov F, Pavlik V, Hnatko M. The effect of electropolishing in a deep eutectic solvent (Ethaline) on the surface properties and corrosion resistance of aluminium-magnesium alloy. Vopr Khimii i Khimicheskoi Tekhnologii 2020. https://doi.org/10.32434/0321-4095-2020-131-4-66-71.

[33] Marola S, Bosia S, Veltro A, Fiore G, Manfredi D, Lombardi M, et al. Residual stresses in additively manufactured AlSi10Mg: Raman spectroscopy and X-ray diffraction analysis. Mater Des 2021. https://doi.org/10.1016/j.matdes.2021.109550.

[34] Uzan NE, Ramati S, Shneck R, Frage N, Yeheskel O. On the effect of shot-peening on

fatigue resistance of AlSi10Mg specimens fabricated by additive manufacturing using selective laser melting (AM-SLM). Addit Manuf 2018. https://doi.org/10.1016/j.addma.2018.03.030.

[35] Wagner L, Mueller C. Effect of shot peening on fatigue behavior in al-alloys. Mater Manuf Process 1992. https://doi.org/10.1080/10426919208947430.

[36] Wagner L, Mhaede M, Wollmann M, Altenberger I, Sano Y. Surface layer properties and fatigue behavior in Al 7075-T73 and Ti-6Al-4V Comparing results after laser peening; Shot peening and ball-burnishing. Int J Struct Integr 2011. https://doi.org/10.1108/17579861111135923.

[37] Galati M. Electron beam melting process. Addit. Manuf., Elsevier; 2021, p. 277–301. https://doi.org/10.1016/B978-0-12-818411-0.00014-8.

[38] Al-Bermani SS, Blackmore ML, Zhang W, Todd I. The Origin of Microstructural Diversity, Texture, and Mechanical Properties in Electron Beam Melted Ti-6Al-4V. Metall Mater Trans A 2010 4113 2010;41:3422–34. https://doi.org/10.1007/S11661-010-0397-X.

[39] Karlsson J, Norell M, Ackelid U, Engqvist H, Lausmaa J. Surface oxidation behavior of Ti-6Al-4V manufactured by Electron Beam Melting (EBM®). J Manuf Process 2015;17:120–6. https://doi.org/10.1016/j.jmapro.2014.08.005.

[40] Lopes AJ, Ramos LC, Saenz D, Morton P, Terrazas CA, Choudhuri A, et al. Analysis of powder removal methods for ebm manufactured TI-6AL-4V parts. Solid Free. Fabr. 2019 Proc. 30th Annu. Int. Solid Free. Fabr. Symp. - An Addit. Manuf. Conf. SFF 2019, 2019, p. 2064–73.

[41] Galati M, Rizza G, Defanti S, Denti L. Surface roughness prediction model for Electron Beam Melting (EBM) processing Ti6Al4V. Precis Eng 2021. https://doi.org/10.1016/j.precisioneng.2021.01.002.

[42] Shakil SI, Hadadzadeh A, Shalchi Amirkhiz B, Pirgazi H, Mohammadi M, Haghshenas M. Additive manufactured versus cast AlSi10Mg alloy: Microstructure and micromechanics. Results Mater 2021. https://doi.org/10.1016/j.rinma.2021.100178.

[43] Aboulkhair NT, Simonelli M, Parry L, Ashcroft I, Tuck C, Hague R. 3D printing of Aluminium alloys: Additive Manufacturing of Aluminium alloys using selective laser melting. Prog Mater Sci 2019;106:100578. https://doi.org/10.1016/j.pmatsci.2019.100578.

[44] Trevisan F, Calignano F, Lorusso M, Pakkanen J, Aversa A, Ambrosio EP, et al. On the selective laser melting (SLM) of the AlSi10Mg alloy: Process, microstructure, and mechanical properties. Materials (Basel) 2017. https://doi.org/10.3390/ma10010076.

[45] Ye H. An overview of the development of Al-Si-alloy based material for engine applications. J Mater Eng Perform 2003. https://doi.org/10.1361/105994903770343132.

[46] Singh P, Pungotra H, Kalsi NS. On the characteristics of titanium alloys for the aircraft applications. Mater. Today Proc., 2017. https://doi.org/10.1016/j.matpr.2017.07.249.

[47] Giannatsis J, Dedoussis V. Additive fabrication technologies applied to medicine and health care: A review. Int J Adv Manuf Technol 2009. https://doi.org/10.1007/s00170-007-1308-1.

[48] Oryshchenko AS, Gorynin I V., Leonov VP, Kudryavtsev AS, Mikhailov VI, Chudakov E V. Marine titanium alloys: Present and future. Inorg Mater Appl Res 2015. https://doi.org/10.1134/S2075113315060106.

[49] Cui C, Hu BM, Zhao L, Liu S. Titanium alloy production technology, market prospects and industry development. Mater Des 2011. https://doi.org/10.1016/j.matdes.2010.09.011.

[50] Liu S, Shin YC. Additive manufacturing of Ti6Al4V alloy: A review. Mater Des 2019. https://doi.org/10.1016/j.matdes.2018.107552.

[51] Calignano F, Iuliano L, Galati M, Minetola P, Marchiandi G. Accuracy of down-facing surfaces in complex internal channels produced by laser powder bed fusion (L-PBF). Procedia CIRP 2020;88:423–6. https://doi.org/10.1016/j.procir.2020.05.073.

[52] SAE International. Procedures for Using Standard Shot Peening Almen Test Strip. 2017. https://doi.org/https://doi.org/10.4271/J443_201708.

[53] Bagherifard S. Enhancing the Structural Performance of Lightweight Metals by Shot Peening. Adv Eng Mater 2019. https://doi.org/10.1002/adem.201801140.

[54] SAE International. SAE J443: Procedures for Using Standard Shot Peening Almen Strip. Surf Veh Recomm Pract 2010.

[55] Ghara T, Paul S, Bandyopadhyay PP. Effect of Grit Blasting Parameters on Surface and Near-Surface Properties of Different Metal Alloys. J Therm Spray Technol 2021. https://doi.org/10.1007/s11666-020-01127-1.

[56] Nagalingam AP, Vohra MS, Kapur P, Yeo SH. Effect of cut-off, evaluation length, and measurement area in profile and areal surface texture characterization of as-built metal additive manufactured components. Appl Sci 2021. https://doi.org/10.3390/app11115089.

[57] Triantaphyllou A, Giusca CL, Macaulay GD, Roerig F, Hoebel M, Leach RK, et al. Surface texture measurement for additive manufacturing. Surf Topogr Metrol Prop 2015. https://doi.org/10.1088/2051-672X/3/2/024002.

[58] Lou S, Jiang X, Sun W, Zeng W, Pagani L, Scott PJ. Characterisation methods for powder bed fusion processed surface topography. Precis Eng 2019. https://doi.org/10.1016/j.precisioneng.2018.09.007.

[59] Fox JC, Moylan SP, Lane BM. Preliminary study toward surface texture as a process signature in laser powder bed fusion additive manufacturing. Proc. - ASPE/euspen 2016 Summer Top. Meet. Dimens. Accuracy Surf. Finish Addit. Manuf., 2016.

[60] Cabrini M, Lorenzi S, Pastore T, Pellegrini S, Manfredi D, Fino P, et al. Evaluation of corrosion resistance of Al-10Si-Mg alloy obtained by means of Direct Metal Laser Sintering. J Mater Process Technol 2016. https://doi.org/10.1016/j.jmatprotec.2015.12.033.

[61] Charles A, Bayat M, Elkaseer A, Thijs L, Hattel JH, Scholz S. Elucidation of dross formation in laser powder bed fusion at down-facing surfaces: Phenomenon-oriented multiphysics simulation and experimental validation. Addit Manuf 2022. https://doi.org/10.1016/j.addma.2021.102551.

[62] Vayssette B, Saintier N, Brugger C, El May M, Pessard E. Numerical modelling of surface roughness effect on the fatigue behavior of Ti-6Al-4V obtained by additive manufacturing. Int J Fatigue 2019. https://doi.org/10.1016/j.ijfatigue.2019.02.014.